Targeting glycolysis in endothelial cells to prevent intraplaque neovascularization and atherogenesis in mice

Perrotta, P.

Chapter 8

Three-dimensional imaging of intraplaque neovascularization in a mouse model of advanced atherosclerosis

Perrotta P, Pintelon I, de Vries M.R, Quax P.H.A, Timmermans J, De Meyer G.R.Y, Martinet W.

*Journal of Vascular Research.*2020 Jul 1;1-7.

Abstract

Multiple lines of evidence suggest that intraplaque (IP) neovascularization promotes atherosclerotic plaque growth, destabilization and rupture. However, pharmacological inhibition of IP neo-vascularization remains largely unexplored due to the limited number of animal models that develop IP neovessels and the lack of reliable methods for visualizing IP angiogenesis. Here, we applied 3D confocal microscopy with an optimized tissue-clearing process, termed iDISCO (immunolabeling-enabled 3D Imaging of Solvent Cleared Organs) to visualize IP neovessels in ApoE$^{-/-}$ mice carrying a heterozygous mutation (C1039+/-) in the fibrillin-1 gene. Unlike regular ApoE$^{-/-}$ mice, this mouse model is characterized by the presence of advanced plaques with evident IP neovascularization. Plaques were stained with antibodies against endothelial marker CD31 for 3 days, followed by incubation with fluorescently labelled secondary antibodies. Subsequent tissue clearing with dichloromethane (DCM)/methanol, DCM and dibenzyl ether allowed easy visualization and 3D reconstruction of the IP vascular network while plaque morphology remained intact.

Introduction

Atherosclerosis is a progressive inflammatory disease that leads to plaque formation at specific sites of the arterial tree [1]. Formation of atherosclerotic plaques typically starts with the deposition of lipids in the intima, followed by endothelial activation and infiltration of macrophages and other inflammatory cells into the subendothelial layer. The first grossly visible vascular lesions, called fatty streaks, transform into more advanced lesions by the migration and proliferation of vascular smooth muscle cells (VSMCs), activation of macrophages and the accumulation of lipid-rich necrotic debris. These plaques typically have a thick fibrous cap consisting of VSMCs and extracellular matrix that encloses a lipid-rich necrotic core [2, 3]. Over time, plaques can become increasingly complex with calcification, ulceration at the luminal surface, and the presence of small neovessels that grow into the lesion from the media of the blood vessel wall. Several stimuli inside the plaque such as hypoxia and high oxidative stress trigger the formation of such intraplaque (IP) neovessels [4]. Growing evidence suggests that IP neovessels are leaky and promote the entry of several plaque components including red blood cells, lipids and inflammatory cells [5], which may accelerate the progression and destabilization of developing plaques [6, 7]. Along these lines, blocking IP angiogenesis has been proposed as a novel approach for decreasing plaque instability and for limiting cardiovascular risk [8, 9]. Apolipoprotein E-deficient ($ApoE^{-/-}$) mice containing a heterozygous mutation (C1039G+/-) in the fibrillin-1 (Fbn1) gene represent a unique mouse model of advanced atherosclerosis with human-like plaque characteristics such as IP neovascularization [10, 11]. Unlike other experimental models of atherosclerosis, $ApoE^{-/-}Fbn1^{C1039G+/-}$ mice show fragmentation of elastic fibers, which facilitates neovessel sprouting from the adventitial vasa vasorum into the plaque [12], similarly to what occurs in human plaques. Conventional immunohistochemistry is currently the gold standard for analysis of plaque composition, yet it does not allow an accurate visualization and quantification of such neovessels inside the complex structure of the plaque. In the present study, we optimized an optical ex vivo clearing method for the visualization of IP angiogenesis in $ApoE^{-/-}Fbn1^{C1039G+/-}$ mice, termed immunolabeling-enabled three-dimensional imaging of solvent–cleared organs (iDISCO)

Materials and Methods

Mice

Female ApoE$^{-/-}$Fbn1$^{C1039G+/-}$ mice were fed a western-type diet (WD) (Altromin, C1000 diet supplemented with 20% milkfat and 0.15% cholesterol, #100171) starting at 8 weeks of age. After 20 weeks on the WD, mice were euthanized with an overdose of sodium pentobarbital (250 mg/kg i.p.) and perfused with 20 mL of 4% paraformaldehyde (PFA) in phosphate-buffered saline (PBS). Carotid arteries were dissected and incubated in 4% PFA in PBS overnight. Standard ApoE$^{-/-}$ mice that did not contain the C1039+/- mutation (but fed WD for 20 weeks) were used as negative controls since they develop plaques without IP neovascularization. All animal procedures were conducted according to the guidelines from Directive 2010/63/EU of the European Parliament on the protection of animals used for scientific purposes. Experiments were approved by the ethics committee of the University of Antwerp.

Immunostaining and iDISCO clearing

Tissue samples were incubated in permeabilization solution (1x PBS, 0.2% Triton X-100, 0.3M glycine, 20% DMSO) overnight. Samples were then washed for 1 hour in 1x PBS/0.2% Tween-20 and incubated in blocking buffer (1xPBS, 0.2% Triton X-100, 10% DMSO, 3% donkey serum) for 8 hours, followed by incubation with primary rat anti-mouse CD31 antibody (Abcam, ab56299; 10 µg/ml) in permeabilization buffer (1x PBS, 0.2% Triton X-100, 0.3M glycine, 20% DMSO) for 72 hours. Finally, samples were washed 3 times in 1xPBS, 0.2% Triton X-100 followed by incubation with goat anti-rat Alexa fluor 546 (Thermo Fisher, A11081; 1:500 dilution) for 48 hours. For nuclear labelling, samples were incubated with DAPI (Sigma-Aldrich, 5 µg/ml) for 30 minutes. Next, immunolabeled samples were dehydrated in a methanol gradient (in PBS) by incubating tissue specimens in 20% methanol (30 min), 50% methanol (30 min), 70% methanol (30 min), and 100% methanol (overnight).

Subsequently, samples were incubated for 2 hours in 66% dichloromethane (DCM)/34% methanol, then washed twice for 15 min in 100% DCM.

Finally, samples were incubated in dibenzyl ether (DBE) until transparency was achieved (approximately 3 hours)

Confocal imaging and histology

Cleared samples were imaged on an inverted Leica TCS SP8 confocal laser scanning microscope, using a 20x/0.75 HC PL Apo objective lens. Samples were positioned in a glass bottom Petri dish and submerged in DBE. DAPI was visualized using a 405 nm diode laser and the Alexa Fluor 546 fluorescence was imaged with the 546 nm wavelength of a white light laser. For each sample, an image stack (z step size ~ 5 µm) with 1024x1024 pixel resolution was captured. Three-dimensional renderings were obtained using Leica LAS X 3D visualisation software. The Imaris image analysis software enabled the specific selection and measurement of the IP blood vessels, by applying a new surface rendering based on the intensity of the fluorescent signal. Following the imaging, samples were embedded in paraffin, cut into 5 µm sections and stained with hematoxylin and eosin (H&E). H&E stains were imaged using an Olympus BX43 microscope.

Results and Discussion

We previously reported that the heterozygous mutation C1039G+/- in the fibrillin-1 (Fbn1) gene leads to advanced unstable atherosclerotic plaques in $ApoE^{-/-}$ mice, a standard mouse model of atherosclerosis [10, 11]. Fbn1 is an extracellular matrix glycoprotein secreted by fibroblasts and incorporated into microfibrils. These fibrillin-rich microfibrils are associated with cross-linked elastin to form mature elastic fibers. Mutations in the Fbn1 gene result in impaired microfibrillar assembly and deposition, followed by fragmentation of elastic fibers. This loss of structural integrity of the vessel wall leads to progressive dilatation and arterial stiffening, resembling vascular ageing [11]. Fragmentation of the elastic fibers gives rise to elastin-derived peptides, which attract monocytes, enhancing the inflammatory reaction in the vessel wall. Moreover, extensive neovascularization is observed in the brachiocephalic and common carotid arteries of $ApoE^{-/-}Fbn1^{C1039G+/-}$ mice fed the WD [12]. These features are rarely seen in murine atherosclerosis models, but are frequently observed in

advanced human plaques. IP neovessels in ApoE$^{-/-}$Fbn1$^{C1039G+/-}$ mice on the WD likely arise from the adventitial vasa vasorum and sprout out of the media into the plaque [9]. Although the exact role of IP neovessels is not exactly understood, it is important to note that such structures are immature and leaky. Indeed, besides being an entry point for leukocytes and lipoproteins, IP neovessels appear to be a source of erythrocytes and platelets inside the plaque, thereby promoting macrophage activation and plaque destabilization.

Imaging of IP neovascularization is possible in human plaques using microvascular imaging and contrast-enhanced ultrasonography [13-16], though this approach is not feasible (or at least unlikely) in mouse plaques due to the extremely small size of the IP neovessels. Hitherto, immunohistochemical analysis of paraffin-embedded sections remains the only method for evaluating IP angiogenesis in mouse plaques. Figure 1 shows representative (immuno)histochemical stains of IP neovessels in plaques of ApoE$^{-/-}$Fbn1$^{C1039G+/-}$ mice. Because both contrast-enhanced ultrasonography and histological analysis of plaques are 2D imaging techniques, they have limitations regarding the interpretation of the “architecture” of microvessel circuits in the atherosclerotic plaque. In recent years, a technique called ‘tissue clearing’ has re-emerged, offering an alternative approach for tissue sectioning. Nowadays numerous protocols allow optical clearing and detailed 3D imaging of intact organs [17-22].

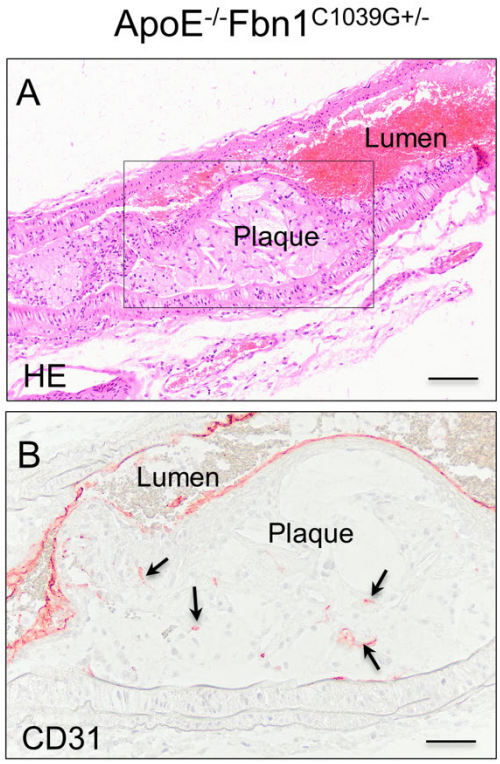

Figure 1. Standard (immuno)histochemical analyses of intraplaque neovascularization in carotid artery plaques from ApoE$^{-/-}$Fbn1$^{C1039G+/-}$ mice that were fed a western diet for 20 weeks. (a) Representative low power micrograph of an H&E stained, paraffin-embedded longitudinal section of carotid plaque. Scale bar = 100µm. (b) Detail of plaque with intraplaque microvessel stain for CD31 (boxed area in panel a) Scale bar = 50 µm.

Immunolabeling-enabled three-dimensional imaging of solvent-cleared organs (iDISCO) combines immunolabeling of large tissue samples for volume imaging with 3DISCO (3D imaging of solvent-cleared organs) [23]. iDISCO is an optical clearing method that makes biological samples more transparent ('cleared') (Figure 2) and has been successfully used to image three-dimensional structures, including intact mouse organs such as brain, kidney, intestine, eye and even whole embryos [21-25]. Recently, Becher et al. [26] applied iDISCO technology for 3D profiling of atherosclerotic plaques and arterial remodeling after carotid artery ligation. We

optimized iDISCO for mouse atherosclerotic tissue using endothelial cell (EC)-specific CD31 antibodies and we show here for the first time a 3D reconstruction of IP neovascularization in carotid plaques of ApoE$^{-/-}$Fbn1$^{C1039G+/-}$ mice. From our experience, the following modifications to the iDISCO protocol were essential for obtaining good visualization of neovessels in carotid plaques: (i) high CD31 antibody concentrations (10 µg/ml) were required for best imaging results, (ii) an overnight incubation step in permeabilizing solution for good tissue penetration of the primary antibody, though we recommend a 72 hour incubation, and (iii) a simple clearing protocol with a mixture of 66% dichloromethane (DCM) and 34% methanol (MeOH), followed by incubation in pure DCM and dibenzyl ether was sufficient to visualize the IP vascular network, in contrast to previously published protocols that are more labor-intensive[17].

Cleared samples of total organs are typically visualized using light sheet microscopy, allowing rapid 3D imaging of these large samples [17-20]. Less thick, cleared specimens can also be imaged by confocal microscopy and hence benefit from the higher resolution that can be obtained [22]. Imaging of cleared segments of the carotid arteries by confocal microscopy resulted in visualization of the delicate IP neovascularization in carotid plaques of ApoE$^{-/-}$Fbn1 $^{C1039G+/-}$ mice and confirmed the labeling of IP neovessels and the complete clearing of the carotid artery segments.

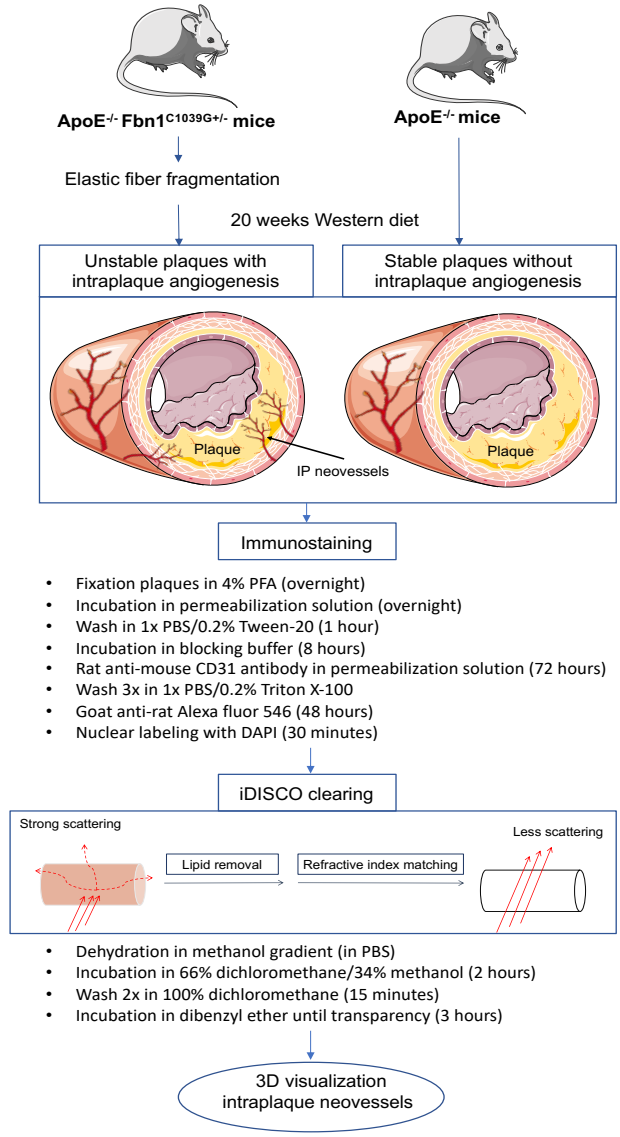

Figure 2. Schematic overview of the different steps required for immunostaining and tissue clearing. Solvent-based tissue clearing is a three-step process. Firstly, the tissue is dehydrated and lipids are removed by sequential incubation in a methanol gradient (20, 50, 70, 100% methanol in distilled water). Secondly, the tissue is transferred to a high refractive index solution where additional lipid solvation and clearing occurs (66% dichloromethane/34% methanol). Finally, the lipid-free tissue sample is placed in a high refractive index matching solution (dibenzyl ether) for further clearing.

Three-dimensional reconstruction (online supplementary video 1) and a z-stack (online supplementary video 2) show the high degree of tortuosity and irregularities in the structure of IP neovessels from ApoE$^{-/-}$Fbn1 $^{C1039G+/-}$ mice, which is not obvious in single plane images of 2D sections (Figure 3). To evaluate the specificity of endothelial CD31 staining in IP angiogenesis, we also applied this technique to regular ApoE$^{-/-}$ mice that develop plaques after being fed the WD, albeit without IP neovascularization. The recorded z-stack shows that CD31 staining did not occur in carotid plaques of ApoE$^{-/-}$ mice (online supplementary video 3), although it was clearly present at the luminal EC layer and in the adventitia (Figure 4).

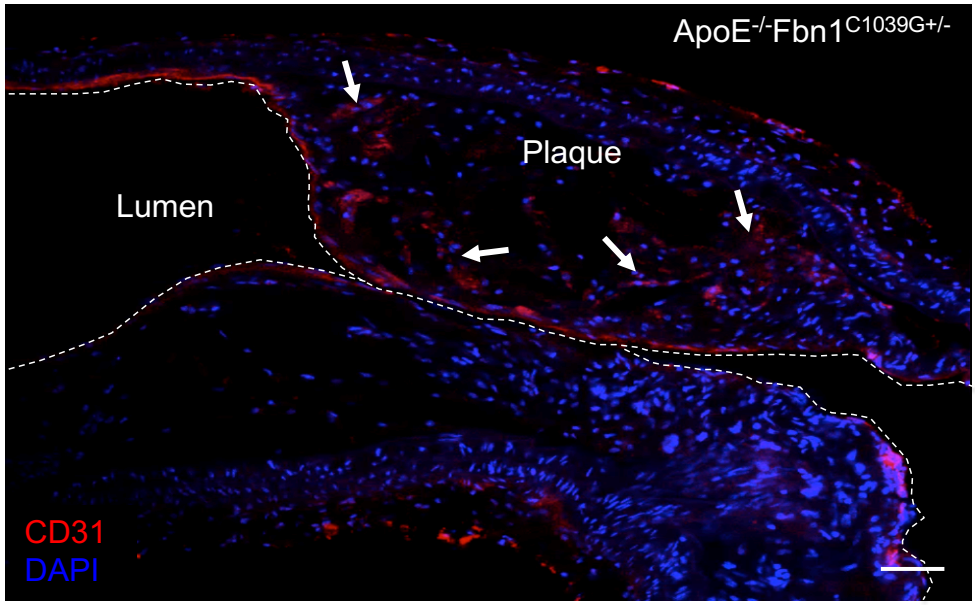

Figure 3. Representative 2D visualization of intraplaque neovascularization in a single z-stack slide of a carotid artery plaque from ApoE$^{-/-}$Fbn1$^{C1039G+/-}$ mice after CD31 immunohistochemical staining and iDISCO clearing. Multiple red-stained CD31 positive endothelial cells are detectable inside the plaque (arrows). Scale bar = 50 µm.

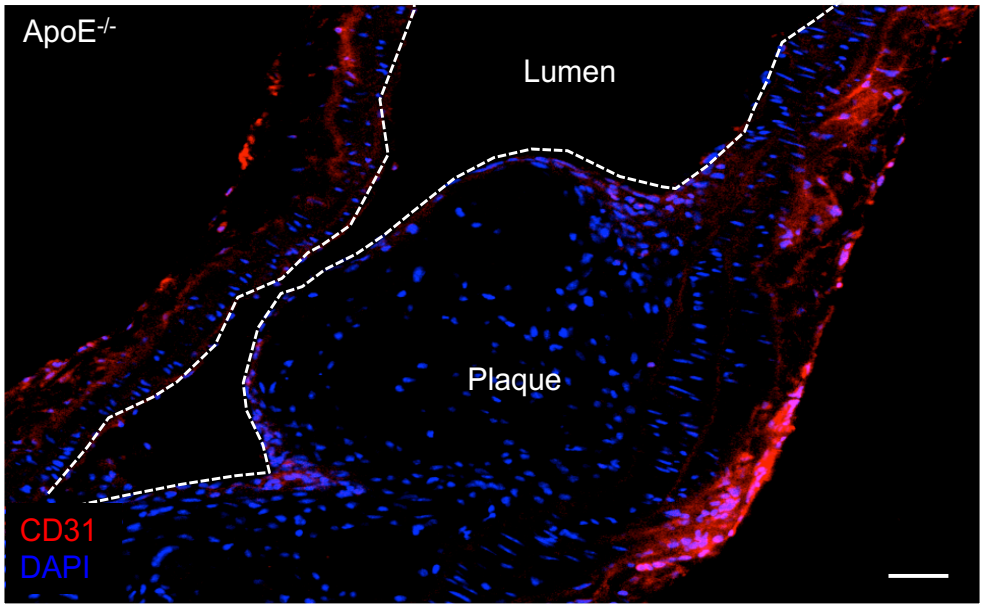

Figure 4. Intraplaque neovascularization is absent in plaques of ApoE$^{-/-}$ mice. A single representative z-stack slide of a plaque in the brachiocephalic artery is shown. CD31 positive cells (red) are not present inside the plaque, but clearly detectable in the intima. Scale bar = 50 µm.

Further analyses of the obtained images demonstrated that the applied technique is not only limited to the visualization of the 3D distribution of the IP neovascularisation (Figure 5A). Using 3D analysis software, neovessels entering the plaque can be selectively depicted in the 3D rendering and quantitative measurements can be obtained (white area in Figure 5B). The total of volume of IP vessels as shown in Figure 5B was calculated to be 0.068 mm^3 and can be used to compare IP angiogenesis between different plaques. Clearing procedures such as 3DISCO lead to substantial shrinkage and might affect tissue morphology [22, 27]. However, the shorter clearing procedure that was used for the carotid segments definitely protected the tissue from the effects of the clearing process, as the structure of the plaque was not altered after clearing. This was confirmed by applying our standard 2D histological techniques on the cleared tissues after imaging, allowing us to examine the structure and composition of the plaque (Figure 6). Moreover,

fluorescent labeling of the tissue was preserved after the clearing process and paraffin embedding (data not shown) allowing re-examination of H&E-stained sections of the paraffin embedded tissue by fluorescence microscopy, if needed.

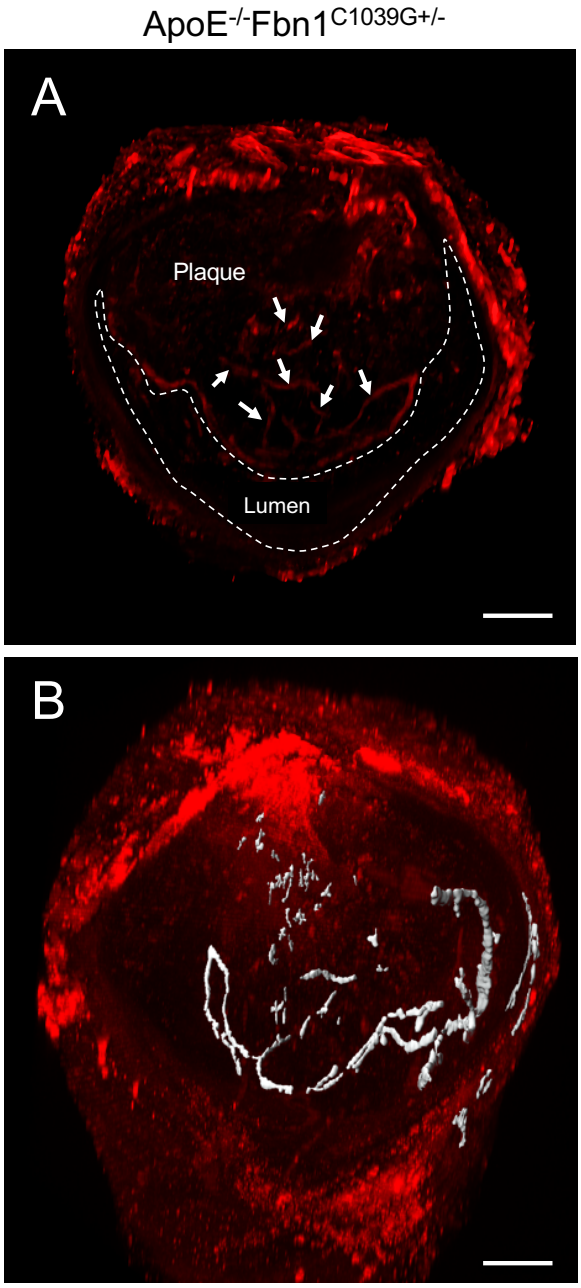

Figure 5. Representative 3D reconstruction of a carotid artery segment (50 z-stack slides) from ApoE$^{-/-}$Fbn1$^{C1039G+/-}$ mice after CD31 immunohistochemical staining and iDISCO clearing. (a) Multiple red-stained CD31 positive endothelial cells are detectable inside the plaque that is bulging the lumen. The 3D reconstruction clearly illustrates the complex distribution of the neovascularisation inside the plaque (white arrows). (b) Using 3D analysis software, neovessels entering the plaque can selectively be depicted (grey) in the 3D image and quantitative measurements such as the total of volume of the IP vessels can be obtained. Scale bar = 80 µm

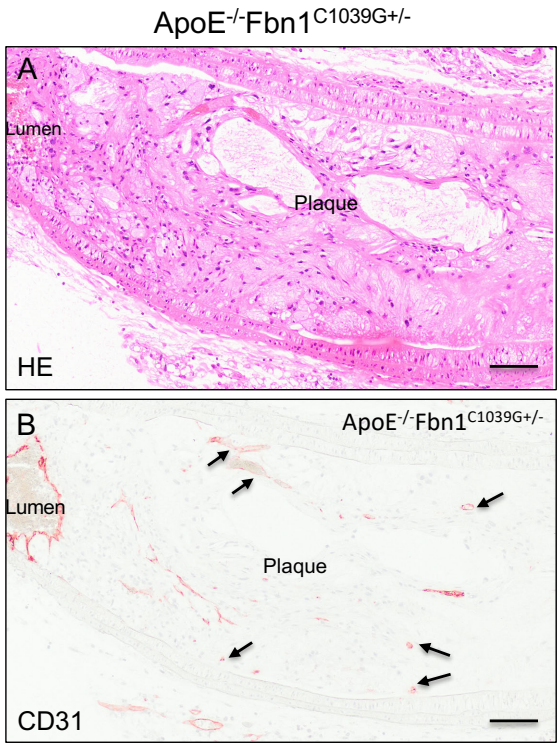

Figure 6. (a-b) Hematoxylin & eosin staining and CD31 immunohistochemical staining of a carotid artery plaque from a representative ApoE$^{-/-}$Fbn1$^{C1039G+/-}$ mouse after iDISCO clearing, showing that the morphology of the plaque and the structure of the neovessels (arrows) were not affected by the clearing procedure. Scale bar = 100 µm.

Clearing and 3D imaging of human artery segments was not performed in this study and might present certain challenges and constraints. Considering the thickness and

composition of human plaques, we expect that the described iDISCO procedure for mouse tissue will need to be adapted, and will become more complex with longer incubation times for dehydration and clearing. Because of their size, 3D imaging of human plaques will require dedicated light sheet microscopy. In addition to the clearing procedure limitations that have already been described by Ali Ertürk et al. [27], such as that this protocol can only be used on fixed tissues and that samples cannot be stored for prolonged periods, the toxicity of the organic solutions used in our protocol might be an extra limitation. Nevertheless, our protocol is straightforward and reproducible which makes it an effective method for visualizing and analyzing neovessels inside atherosclerotic plaques.

In conclusion, this is the first report to apply iDISCO technology to atherosclerotic blood vessels and it provides a simple, inexpensive and effective method for visualizing and reconstructing, in three dimensions, the presence of IP neovessels inside these lesions. This could be a useful new tool for studies aimed at determining whether there is a causal relationship between the presence of neovessel structures and atherogenesis or between angiogenic stimuli and plaque angiogenesis.

Online supplemental material

Video 1. Representative 3D reconstruction of a carotid artery segment (50 z-stack slides) in ApoE$^{-/-}$Fbn1$^{C1039G+/-}$ mice stained with the endothelial marker CD31. For a general overview of the different parts of the vessel, we refer to a single frame of this video in Figure 5A.

Video 2. Video showing all confocal planes from a z-stack taken from a carotid artery segment of a representative ApoE$^{-/-}$Fbn1$^{C1039G+/-}$ mouse. DAPI (blue) was used to stain the nuclei and CD31 (red) visualizes the endothelial cells.

Video 3. Video showing all confocal planes from a z-stack taken from a brachiocephalic artery segment of a representative ApoE$^{-/-}$ mouse, confirming that there is no CD31 (red) staining present inside the plaque. Nuclei are stained with DAPI (blue).

Acknowledgement

The authors would like to thank Rita Van den Bossche, Mandy Vermont, Dominique De Rijck and Gleison D.P. Bossolani for technical help. The authors are grateful to Dr. Bronwen Martin for critical reading of the manuscript.

Statement of Ethics

All animal procedures were conducted according to the guidelines from Directive 2010/63/EU of the European Parliament on the protection of animals used for scientific purposes. Experiments were approved by the ethics committee of the University of Antwerp.

Disclosure Statement

The authors have no conflicts of interest to declare.

Funding Sources

This work was supported by the University of Antwerp (DOCPRO-BOF) and the Horizon 2020 program of the European Union – Marie Sklodowska Curie actions – ITN – MOGLYNET [grant number 675527]. The Leica SP 8 (Hercules grant AUHA.15.12) confocal microscope was funded by the Hercules Foundation of the Flemish Government.

Author Contributions

Paola Perrotta, Isabel Pintelon and Wim Martinet: study conception and design
Paola Perrotta, Isabel Pintelon and Margreet R. De Vries: acquisition of data
All authors contributed to the analysis and interpretation of data. All authors also helped drafting the manuscript and approved the final version of the manuscript.

References

1. Ross R. Atherosclerosis is an inflammatory disease. *Am Heart J*. 1999;138:S419-420
2. Moreno PR, Sanz J, Fuster V. Promoting mechanisms of vascular health: Circulating progenitor cells, angiogenesis, and reverse cholesterol transport. *J Am Coll Cardiol*. 2009;53:2315-2323
3. Bentzon JF, Otsuka F, Virmani R, Falk E. Mechanisms of plaque formation and rupture. *Circ Res*. 2014;114:1852-1866
4. Moreno PR, Purushothaman KR, Sirol M, Levy AP, Fuster V. Neovascularization in human atherosclerosis. *Circulation*. 2006;113:2245-2252
5. de Vries MR, Quax PH. Plaque angiogenesis and its relation to inflammation and atherosclerotic plaque destabilization. *Curr Opin Lipidol*. 2016;27:499-506
6. Stary HC, Chandler AB, Dinsmore RE, Fuster V, Glagov S, Insull W, Jr., Rosenfeld ME, Schwartz CJ, Wagner WD, Wissler RW. A definition of advanced types of atherosclerotic lesions and a histological classification of atherosclerosis. A report from the committee on vascular lesions of the council on arteriosclerosis, american heart association. *Circulation*. 1995;92:1355-1374
7. Nakamura J, Nakamura T, Deyama J, Fujioka D, Kawabata K, Obata JE, Watanabe K, Watanabe Y, Kugiyama K. Assessment of carotid plaque neovascularization using quantitative analysis of contrast-enhanced ultrasound imaging is useful for risk stratification in patients with coronary artery disease. *Int J Cardiol*. 2015;195:113-119
8. Parma L, Baganha F, Quax PHA, de Vries MR. Plaque angiogenesis and intraplaque hemorrhage in atherosclerosis. *Eur J Pharmacol*. 2017;816:107-115
9. Perrotta P, Emini Veseli B, Van der Veken B, Roth L, Martinet W, De Meyer GRY. Pharmacological strategies to inhibit intraplaque angiogenesis in atherosclerosis. *Vascul Pharmacol*. 2019;112:72-78

10. Van Herck JL, De Meyer GR, Martinet W, Van Hove CE, Foubert K, Theunis MH, Apers S, Bult H, Vrints CJ, Herman AG. Impaired fibrillin-1 function promotes features of plaque instability in apolipoprotein e-deficient mice. *Circulation*. 2009;120:2478-2487
11. Van der Donckt C, Van Herck JL, Schrijvers DM, Vanhoutte G, Verhoye M, Blockx I, Van Der Linden A, Bauters D, Lijnen HR, Sluimer JC, Roth L, Van Hove CE, Fransen P, Knaapen MW, Hervent AS, De Keulenaer GW, Bult H, Martinet W, Herman AG, De Meyer GR. Elastin fragmentation in atherosclerotic mice leads to intraplaque neovascularization, plaque rupture, myocardial infarction, stroke, and sudden death. *Eur Heart J*. 2015;36:1049-1058
12. Emini Veseli B, Perrotta P, De Meyer GRA, Roth L, Van der Donckt C, Martinet W, De Meyer GRY. Animal models of atherosclerosis. *Eur J Pharmacol*. 2017;816:3-13
13. Coli S, Magnoni M, Sangiorgi G, Marrocco-Trischitta MM, Melisurgo G, Mauriello A, Spagnoli L, Chiesa R, Cianflone D, Maseri A. Contrast-enhanced ultrasound imaging of intraplaque neovascularization in carotid arteries: Correlation with histology and plaque echogenicity. *J Am Coll Cardiol*. 2008;52:223-230
14. Cattaneo M, Staub D, Porretta AP, Gallino JM, Santini P, Limoni C, Wyttenbach R, Gallino A. Contrast-enhanced ultrasound imaging of intraplaque neovascularization and its correlation to plaque echogenicity in human carotid arteries atherosclerosis. *Int J Cardiol*. 2016;223:917-922
15. Oura K, Kato T, Ohba H, Terayama Y. Evaluation of intraplaque neovascularization using superb microvascular imaging and contrast-enhanced ultrasonography. *J Stroke Cerebrovasc Dis*. 2018;27:2348-2353
16. Andrews JPM, Fayad ZA, Dweck MR. New methods to image unstable atherosclerotic plaques. *Atherosclerosis*. 2018;272:118-128
17. Richardson DS, Lichtman JW. Clarifying tissue clearing. *Cell*. 2015;162:246-257
18. Richardson DS, Lichtman JW. Snapshot: Tissue clearing. *Cell*. 2017;171:496-496 e491

19. Ariel P. A beginner's guide to tissue clearing. *Int J Biochem Cell Biol*. 2017;84:35-39
20. Orlich M, Kiefer F. A qualitative comparison of ten tissue clearing techniques. *Histol Histopathol*. 2018;33:181-199
21. Vogt N. Transparency in large tissue samples. *Nat Methods*. 2015;12:11
22. Bossolani GDP, Pintelon I, Detrez JD, Buckinx R, Thys S, Zanoni JN, De Vos WH, Timmermans JP. Comparative analysis reveals ce3d as optimal clearing method for in toto imaging of the mouse intestine. *Neurogastroenterol Motil*. 2019;31:e13560
23. Renier N, Wu Z, Simon DJ, Yang J, Ariel P, Tessier-Lavigne M. Idisco: A simple, rapid method to immunolabel large tissue samples for volume imaging. *Cell*. 2014;159:896-910
24. Henning Y, Osadnik C, Malkemper EP. Eyeci: Optical clearing and imaging of immunolabeled mouse eyes using light-sheet fluorescence microscopy. *Exp Eye Res*. 2019;180:137-145
25. Walter A, van der Spek L, Hardy E, Bemelmans AP, Rouach N, Rancillac A. Structural and functional connections between the median and the ventrolateral preoptic nucleus. *Brain Struct Funct*. 2019
26. Becher T, Riascos-Bernal DF, Kramer DJ, Almonte V, Chi J, Tong T, Oliveira-Paula GH, Koleilat I, Chen W, Cohen P, Sibinga NE. Three-dimensional imaging provides detailed atherosclerotic plaque morphology and reveals angiogenesis after carotid artery ligation. *Circ Res*. 2020
27. Erturk A, Becker K, Jahrling N, Mauch CP, Hojer CD, Egen JG, Hellal F, Bradke F, Sheng M, Dodt HU. Three-dimensional imaging of solvent-cleared organs using 3disco. *Nat Protoc*. 2012;7:1983-1995